Photochemistry and Photobiology, 2005, 81: 242–249

# Photodynamic Characterization and *In Vitro* Application of Methylene Blue-containing Nanoparticle Platforms¶

**Wei Tang[1], Hao Xu[2], Raoul Kopelman*[1] and Martin A. Philbert[2]**

[1]Department of Chemistry, University of Michigan, Ann Arbor, MI
[2]Department of Environmental Health Sciences, University of Michigan, Ann Arbor, MI

**Received 22 October 2004; accepted 30 November 2004**

## ABSTRACT

**This article presents the development and characterization of nanoparticles loaded with methylene blue (MB), which are designed to be administered to tumor cells externally and deliver singlet oxygen ($^1O_2$) for photodynamic therapy (PDT), *i.e.* cell kill via oxidative stress to the membrane. We demonstrated the encapsulation of MB, a photosensitizer (PS), in three types of sub-200 nm nanoparticles, composed of polyacrylamide, sol–gel silica and organically modified silicate (ORMOSIL), respectively. Induced by light irradiation, the entrapped MB generated $^1O_2$, and the produced $^1O_2$ was measured quantitatively with anthracene-9,10-dipropionic acid, disodium salt, to compare the effects of different matrices on $^1O_2$ delivery. Among these three different kinds of nanoparticles, the polyacrylamide nanoparticles showed the most efficient delivery of $^1O_2$, but its loading of MB was low. In contrast, the sol–gel nanoparticles had the best MB loading but the least efficient $^1O_2$ delivery. In addition to investigating the matrix effects, a preliminary *in vitro* PDT study using the MB-loaded polyacrylamide nanoparticles was conducted on rat C6 glioma tumor cells with positive photodynamic results. The encapsulation of MB in nanoparticles should diminish the interaction of this PS with the biological milieu, thus facilitating its systemic administration. Furthermore, the concept of the drug-delivering nanoparticles has been extended to a new type of dynamic nanoplatform (DNP) that only delivers $^1O_2$. This DNP could also be used as a targeted multifunctional platform for combined diagnostics and therapy of cancer.**

## INTRODUCTION

Photodynamic therapy (PDT) has emerged as a promising method for overcoming some of the inherent problems in classical cancer therapies (1–5). It involves the selective delivery of photosensitizers (PS), such as Photofrin, to tumors. When excited with an appropriate wavelength of visible or near-infrared light, the PS produces singlet oxygen ($^1O_2$) and other reactive oxygen species, resulting in irreversible damage to tumor cells, with minimal systemic toxicity.

An ideal PS for PDT should satisfy several criteria: chemical purity, tumor selectivity and minimal dark toxicity, followed by rapid system clearance, high photochemical reactivity and activation at wavelengths that penetrate deep into tissues (4). Unfortunately, currently available PS only partially fulfill these criteria. First-generation PS such as Photofrin® I, hematoporphyrin derivative and Photofrin® II suffer from several drawbacks (5). They are a complex mixture of several partially unidentified porphyrins, and they also show relatively poor selectivity in terms of target tissue–healthy tissue ratios. In addition, their low extinction coefficients require the administration of large amounts of the drug to obtain a satisfactory phototherapeutic response. Furthermore, their absorption maximum is at a relatively short wavelength (630 nm), leading to poor tissue penetration of light. Finally, these clinically useful compounds readily accumulate in the skin, which upon exposure to light produce a range of adverse dermal effects that persist for up to 4–6 weeks after treatment.

The limitations of Photofrin have encouraged the development of many second-generation PS. Many new PDT drugs have been investigated including porphyrins, chlorins and phthalocyanines, all with favorable PDT properties (6). One of the traditional PS that has been used for a variety of applications, including PDT, is methylene blue (MB) (4,7). We note that intravenous administration of MB is Food and Drug Administration (FDA) approved for methemoglobinemia. Its chemical structure is shown in Fig. 1. Its high quantum yield of $^1O_2$ generation ($\Phi_\Delta \sim 0.5$) (8) in the therapeutic window (600–900 nm), coupled with its low toxicity, has led to the testing of MB as a promising candidate for PDT of cancer (9). It has been found that MB exhibited phototoxicity toward a variety of tumor cell lines *in vitro* (10,11). Recently, local administration of MB was also successfully used in the intratumoral treatment of inoperable esophageal tumors (12). However, clinical use of MB has been limited because of the lack of activity when applied systematically. The weak pharmaceutical effect (10,13,14) results in part from poor penetration of MB into the cellular compartment of the tumor. In addition, once in the biological environment, MB is usually inactivated via the reduction of the cation to the neutral leuko-

¶Posted on the website on 13 December 2004
*To whom correspondence should be addressed: Department of Chemistry, University of Michigan, 930 N. University Avenue, Ann Arbor, MI 48109-1055, USA. Fax: 734-936-2778; e-mail: kopelman@umich.edu

*Abbreviations:* ADPA, anthracene-9,10-dipropionic acid, disodium salt; AM, acetoxymethyl ester; AOT, dioctyl sulfosuccinate; APS, ammonium persulfate; BIS, *N, N'*-methylenebis(acrylamide); Brij 30, polyoxyethylene (4) lauryl ether; DNP, dynamic nanoplatform; FDA, Food and Drug Administration; LMB, leukomethylene blue; MB, methylene blue; MDR, multidrug resistance; MOPS, (3-(*N*-morpholino) propanesulfonic acid) sodium salt; MRI, magnetic resonance imaging; MTMS, methyltrimethyoxysilane; $^1O_2$, singlet oxygen; ORMOSIL, organically modified silicate; PDT, photodynamic therapy; PI, propidium iodide; PS, photosensitizer; PTMS, phenyltrimethyoxysilane; SEM, scanning electron microscopy; TEMED, *N,N,N',N'*-tetramethylethylenediamine; TEOS, tetraethylorthosilicate.

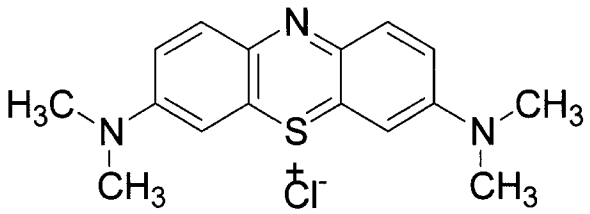

**Figure 1.** Structure of methylene blue (MB).

methylene blue (LMB), which has negligible photodynamic activity (14–16).

Therefore, the major obstacle to the PDT application of MB, which is also a common problem among many other PS, is the difficulty in preparing pharmaceutical formulations that enable their facile administration. To address this issue different strategies have been investigated, which mainly include polymer–PS conjugation as well as encapsulation of the drug in colloidal carriers such as liposomes, oil dispersions and polymeric particles (17). Unfortunately, little investigation has been conducted using drug delivery carriers with MB, although there has been much effort focused on the synthesis or modification of MB (10,11,16).

In recent years, nanoparticles have received increasing attention as a possible means of delivering PDT agents (17,18). However, most of the previous studies (19–23) involved the controlled release of a PS. As a result, the traditional delivery systems suffer from phototoxic side effects due to the posttreatment accumulation of the free PS in the skin and the eyes (24).

These disadvantages have prompted our development of a dynamic nanoplatform (DNP) (25–29), as shown in Fig. 2, which enables the use of PDT methods that differ from conventional approaches. Instead of releasing PS to the inside of cancer cells, the DNP described in this paper is designed to target the cell membranes externally and deliver only $^1O_2$, rather than the PS itself. Thus, this porous nanoparticle-based drug carrier system not only prevents the PS from being pumped back out of the cells by multidrug resistance (MDR) mechanisms but also solves the problem of the free PS's posttreatment accumulation. The DNP is also superior to others by protecting the embedded PS from direct interaction with cellular components. The semipermanent encapsulation of the PS decreases the artifacts that result from erroneous interactions or toxic complications, hence widening the choice of PS to pharmaceutical "reject" molecules such as MB, which would otherwise be unlikely candidates for clinical tumor treatment. Furthermore, such a DNP is a modular system that contains a high degree of loading of photodynamic molecules. This concentrated (critical mass) packaging can be coupled with other incorporated sensitizers, probes or antibodies that together function as a synergistic unit for enhanced therapeutic efficacy. For example, incorporated magnetic resonance imaging (MRI) contrast agents have been reported to assist in on-site tumor detection (30,31). In addition, the surface modification of these nanoparticles is flexible. The most commonly used modification is the use of hydrophilic coatings by PEGylation, which can reduce uptake by the reticuloendothelial system (29,32). Moreover, a variety of monoclonal antibodies and other ligands can be attached to the surface of the nanoparticles as well, to target them to desired sites *in vivo* (33). Present DNP systems in this laboratory (29) use the FDA-approved PDT agent, Photofrin. This study emphasizes the potential use, as a viable substitute to Photofrin, of a simpler and more efficient PS, namely MB, which is likely to gain FDA approval because of its other approved medical applications (4).

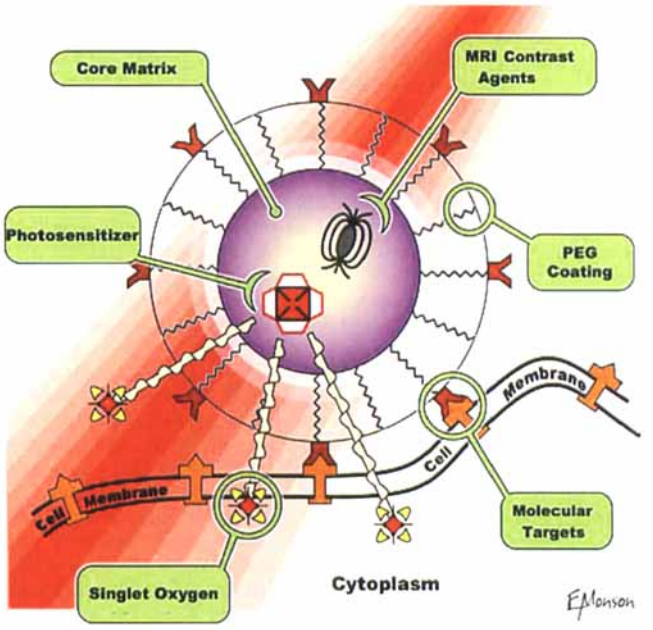


**Figure 2.** Schematic of dynamic nanoplatform (DNP).

The aim of this study is to determine whether MB can be used effectively for the DNP design mentioned above and ultimately for clinical PDT. In this study, MB was encapsulated into three types of nanoparticles: polyacrylamide, sol–gel silica and organically modified silicate (ORMOSIL). On light irradiation, the entrapped MB generated $^1O_2$ and a significant amount of the latter diffused out of the matrix. In addition, the efficiency of $^1O_2$ delivery of these MB-loaded nanoparticles was compared with that of free MB. To evaluate the photocytotoxicity of these nanoparticles, *in vitro* PDT experiments were subsequently conducted on rat C6 glioma tumor cells. Considering the primary importance of particle suspendability in an aqueous environment, the polyacrylamide nanoparticles were selected for the preliminary *in vitro* studies. The results show that irradiation with red light induced a disruption of cell membranes. Thus, the fundamental characterization of MB-loaded nanoparticles has been demonstrated for its potential application in PDT.

## MATERIALS AND METHODS

### Chemicals

MB, the commercially available photosensitizing agent, was acquired from Aldrich (Milwaukee, WI) (certified 97% dye content) without further purification. Acrylamide, *N,N'*-methylenebis(acrylamide) (BIS), *N,N,N',N'*-tetramethylethylenediamine (TEMED), polyoxyethlyene (4) lauryl ether (Brij 30), dioctyl sulfosuccinate (AOT), tetraethylorthosilicate (TEOS), phenyltrimethyoxysilane (PTMS), methyltrimethyoxysilane (MTMS) and ammonia were also purchased from Aldrich. Ammonium persulfate (APS) and (3-(*N*-morpholino) propanesulfonic acid) sodium salt (MOPS) were purchased from Sigma Chemical Co. (St. Louis, MO). Ethanol (200 proof) was obtained from Pharmco Products Inc. (Brookfield, CT) and hexane from Fisher (Fair Lawn, NJ). Anthracene-9,10-dipropionic acid, disodium salt (ADPA) was purchased from Molecular Probes (Eugene, OR). A stock solution of 10 μ*M* ADPA was made in water and kept in the dark until use. All solutions were prepared from 18 MΩ water purified by a Barnstead 1 Thermolyne Nanopure II system. For all aqueous experiments, 0.1 *M* MOPS (pH 7.2) buffer solution was prepared.

### Preparation of nanoparticles loaded with MB

*Polyacrylamide nanoparticles preparation.* The polymerization procedure of acrylamide was similar to that described in previous studies (34,35). The

polymerization solution consisted of 0.9 g acrylamide, 0.27 g BIS and 3 mL of 0.1 *M* MOPS buffer. A 1.8 mL portion of this solution was added to a flask containing 43 mL deoxygenated hexane, 1.6 g AOT, and 3.1 g Brij 30. Once the mixture emulsified, 200 μL of freshly prepared MB solution (20 mg/mL) was added before the polymerization was initiated with 30 μL of 10% (wt/vol) APS and 15 μL of TEMED. The solution was then stirred under argon at room temperature for 2 h. After the reaction, hexane was removed by rotary evaporation, and the particles were precipitated by addition of ethanol. The surfactant, unreacted monomers and excess dye molecules were washed away from the particles with ethanol in an Amicon ultrafiltration cell (Millipore Corp., Bedford, MA), using a 100 kDa filter membrane under 15 psi. The particle suspension was then collected by a suction filtration system (Fisher, Pittsburgh, PA) with a 0.02 μm Whatman Anodisc filter membrane. The MB-loaded nanoparticle formulations were protected from light during the production process.

*Sol–gel silica nanoparticles preparation.* The sol–gel silica nanoparticles were made via a modified Stöber method (32,36,37). The typical reaction solution consists of methanol (99.9%, 24 mL), ammonium hydroxide (30% wt of ammonia, 6 mL) and MB solution (20 mg/mL, 80 μL). On mixing the solution by vigorous magnetic stirring, TEOS (99.9%, 0.2 mL) was added dropwise to initiate the hydrolysis reaction. The resulting solution was stirred at room temperature for approximately 2 h before it was transferred to the Amicon ultrafiltration cell, where it was rinsed rigorously with distilled water and ethanol to ensure removal of all unreacted reactants. The particle suspension was finally passed through the suction filtration system with a 0.02 μm filter membrane and dried to yield an end product of MB-loaded silica nanoparticles.

*ORMOSIL nanoparticles preparation.* The reported procedure (38,39) of the formation of ORMOSIL was adopted to make the MB-loaded nanoparticles. The ORMOSIL nanoparticles were synthesized using two precursors, PTMS and MTMS, which resulted in a hydrophobic outer shell as well as a hydrophilic inner core. Thirty milliliters of deionized water and 38 μL $HNO_3$ was placed in a 50 mL round bottom flask and held at a constant temperature of 60°C in a water bath. Four-hundred microliters of MB (2 mg/mL) was added, and the resultant mixture was stirred at a rate of 1000 rpm. Then, 0.08 mL of PTMS was added for the hydrolysis reaction. After 20 min, 6 mL of ammonium hydroxide was added, and the solution was stirred for 1.5 h or until the solution became milky. MTMS (0.16 mL) was added, and the system was stirred for an additional hour. The resulting particle suspension was suction filtered through the suction filtration system with a 0.1 μm Osmonics/MSI MAGNA Nylon membrane filter. The collected nanoparticles were rinsed several times with water and then resuspended in a 1:1 water–ethanol mixture, sonicated for 30 min. Finally, the MB-loaded ORMOSIL nanoparticles were collected with a 0.02 μm filter membrane and allowed to air-dry.

### Scanning electron microscopy imaging

To prepare the samples for scanning electron microscopy (SEM) studies, dried MB-loaded nanoparticles were dispersed in water, and the resultant suspensions were sonicated for 30 min to prevent aggregation of particles. A drop of each particle suspension was placed on the SEM specimen mount (aluminum) and dried gradually at room temperature. The samples were then sputter coated with gold and observed using a Philips XL30FEG SEM to assess the particle size and shape.

### Spectroscopic characterization

A UV160U UV–visible recording spectrophotometer (Shimadzu, Columbia, MD) was used for absorption measurements. Fluorescence measurements were taken on a FluoroMax-3 Spectrofluorometer (Jobin Yvon/SPEX Division, Instruments S. A. Inc., Edison, NJ) controlled by DataMax spectroscopy software. The approximate amount of MB in the nanoparticles was evaluated by its absorption. The scattering effect of the nanoparticles was removed to a large extent by subtracting the background of the corresponding blank nanoparticles. All spectroscopic experiments on both MB-free dye and MB-loaded nanoparticles were carried out in pH 7.2 MOPS buffer under constant stirring. Each experiment was carried out in triplicate to ensure consistency.

### ADPA test for $^1O_2$

Measurements were carried out in plastic cuvettes (10 × 10 mm) according to a procedure described previously (40,41). In brief, a 2.5 mL MB dye solution or MB-loaded nanoparticle suspension in buffer was mixed with 20 μL ADPA (100 μ*M*) in a cuvette. The solution was irradiated at 650 nm for the $^1O_2$ generation with a slit width of 10 nm using a 150 W ozone-free xenon-arc lamp (Jobin Yvon) while under constant stirring at a moderate speed to ensure better suspension and oxygen diffusion. The fluorescence emission of ADPA excited at 376 nm was collected at different time scales (0, 5, 15 and 30 min).

The $^1O_2$ production of the MB-loaded nanoparticles was determined by using this ADPA method (40). The following equations are tailored specifically to the system we are dealing with, in which a substrate (*i.e.* ADPA) and a sensitizer (*i.e.* MB) are irradiated together in a solution. Hypothetically, the following processes may take place (41):

$$MB + h\nu \rightarrow MB^* \qquad I^{abs} \quad (1)$$

$$MB^* + {}^3O_2 \rightarrow MB + {}^1O_2 \qquad k \quad (2)$$

$$ADPA + {}^1O_2 \rightarrow ADPA\ endoperoxide \qquad k_c \quad (3)$$

$$^1O_2 \rightarrow {}^3O_2 \qquad k_d \quad (4)$$

Here $k$ is the rate constant for the quenching of excited MB by triplet oxygen to produce $^1O_2$; $k_c$ is the rate constant of chemical quenching of $^1O_2$ in the presence of ADPA; however, the $^1O_2$ molecule also decays to the ground state by energy transfer to the solvent or to other species in solution, with a rate constant $k_d$.

A rough estimation of the rate constant for the chemical quenching of ADPA by $^1O_2$ can be obtained using a simplification in which $[^1O_2]$ is independent of [ADPA]. According to Eq. 3, the loss of ADPA in reaction with $^1O_2$ is given by

$$-d[ADPA]/dt = k_c[ADPA][^1O_2] = k[ADPA]$$

where $k = k_c[^1O_2] = \Phi^{^1O_2} I^{abs} k_c/k_d$. Thus, the decay of [ADPA] follows first-order kinetics.

$$[ADPA]_t = [ADPA]_0 \exp(-kt) \quad (5)$$

$$\ln([ADPA]_t/[ADPA]_0) = -kt \quad (6)$$

Therefore, the relative rate constant $k$ can be extrapolated by a linear fit using the experimental points.

### Cell culture

Rat C6 glioma cells were cultured in Dulbecco modified Eagle medium containing 400 mg/L D-glucose, 2 m*M* L-glutamine, 10% fetal bovine serum, 0.3% penicillin, streptomycin and neomycin and incubated at 37°C in a 5% $CO_2$ environment. Cells were plated on uncoated 22 mm glass cover slips 2 days before experimentation.

### *In vitro* PDT studies

The glass cover slips with rat C6 glioma cells on them were removed from the culture medium, rinsed carefully with 1× Hanks balanced salt solution and placed in the microscope chamber at 37°C. The cells were covered with 2 mL 1× Hanks balanced salt solution containing 10 m*M* pH buffer 4-(2-hydroxyethyl)piperazine-1-ethanesulfonic acid, 0.1 μ*M* calcein acetoxymethyl ester (AM), 10 μ*M* propidium iodide (PI) and 1 mg/mL MB-loaded polyacrylamide nanoparticles. Calcein AM, a cell-permeant dye, was used to determine cell viability both before and after PDT. In live cells, the nonfluorescent calcein AM is converted to a green fluorescent calcein, after acetoxymethyl ester hydrolysis by intracellular esterases. Meanwhile, PI marks the nuclei once the integrity of the cell membrane is compromised, *i.e.* detecting dead or dying cells. Cell images were acquired with a Perkin Elmer UltraView confocal microscope system equipped with an argon–krypton laser. Preexposure images were taken with an oil-immersion 60× objective lens in two channels (488 nm excitation of the calcein converted from calcein AM, 568 nm excitation of the PI). The cells were exposed for 5 min at 647 nm resulting in an optical energy dose of ~52 J/cm$^2$. Afterward, images were taken every 2 min, for up to 2 h, to monitor cell death. Finally, a 20× objective was used to broaden the field of view and allow concurrent comparison of the cells exposed to light along with those that had not been exposed.

## RESULTS AND DISCUSSION

### Preparation and characterization of MB-loaded NP

With the aim of solving the problems related to the traditional PS, three kinds of MB-containing nanoparticles were synthesized. The

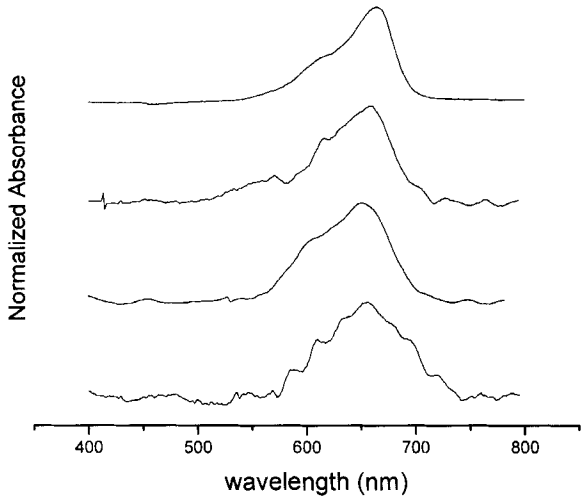


**Figure 3.** Normalized typical absorption spectra of MB-free dye and MB-loaded nanoparticles. From top to bottom: MB-free dye, MB-loaded polyacrylamide nanoparticles, sol–gel silica nanoparticles and ORMOSIL nanoparticles.

choice of loading conditions was dictated by the characteristics of both MB and the nanoparticle matrices. MB is a hydrophilic PS with low molecular weight; thus, polymer matrices with favorable properties were chosen: polyacrylamide, sol–gel silica and ORMOSIL. The optimal parameters for the preparation of these sub-200 nm, MB-loaded nanoparticles were determined on the basis of previous studies (32,35,37,38), with additional adjustments to the concentration of MB. The encapsulation of MB into these varied matrices was demonstrated by the yield of blue powders obtained after washing, as well as by the characteristic absorption peak of MB monomers at 664 nm in the spectra of the product (Fig. 3).

In addition to verifying the encapsulation of MB, the size of each type of MB-loaded, spherical nanoparticles was evaluated by SEM, with typical images shown in Fig. 4. The average diameter of this batch of sol–gel silica nanoparticles was 190 nm, whereas that of the ORMOSIL nanoparticles was 160 nm. Compared with these two silica-based nanoparticles, the polyacrylamide nanoparticles are much smaller in size, mostly in the range of 20–30 nm diameter. The final size of such a nanoparticle is critical for its PDT efficacy, which is highly dependent on the delivery of produced $^1O_2$, the main reactive species liable for photocytotoxicity. The lifetime of $^1O_2$ in aqueous media is in the microsecond regime, during which interval it can migrate on the order of 100 nm (40,41). According to this calculation, the size diversity between the sub-200 nm nanoparticles should have a negligible effect on $^1O_2$ delivery under our experimental conditions. However, because of the complicating effects of the microenvironments inside the nanoparticles, for example, the local oxidation opportunities for the produced $^1O_2$, a study on each individual matrix may be necessary to find the critical radius at which a significant fraction of the produced $^1O_2$ is lost inside the particle as a result of the enhanced reaction with its medium. However, we note that the organic hydrogel particles are quite small (20–30 nm) and mostly filled with water, whereas the larger sol–gel silica or ORMOSIL particles (150–200 nm) consist totally or mostly of inert silica, *i.e.* a medium that is probably not more reactive than water. In any case, related PDT studies (27,29) with Photofrin inside 30–60 nm polyacrylamide particles have shown that the ensuing $^1O_2$ kills cells effectively both *in vitro* and *in vivo*. The drug-loaded nanoparticles are directly targeted to the cell membrane; thus, the required diffusion distance to membrane proteins is only on the nanometer scale. Therefore, the shortened lifetime of $^1O_2$ in biological environments (42) does not seem to affect much the cell killing efficiency in this case.

## Loading of MB

To increase drug loading, the preparation of the MB-loaded nanoparticles was conducted with excess amounts of MB in the reaction solutions. This should minimize the effect of the initial concentration of MB so that other factors such as polymer hydrophilicity and particle size, which contribute to variations in drug loading, can be evaluated. Each matrix is characterized by diverse polymer properties; therefore, the matrices demonstrated markedly different degrees of loading of MB monomers, as estimated by optical absorption data (Fig. 6). The polyacrylamide nanoparticles are hydrophilic but small, resulting in a lower loading of MB compared with the other two larger particles. The sol–gel silica nanoparticles are spacious and negatively charged, which leads to the best loading of the positively charged MB, whereas the ORMOSIL nanoparticles have a unique structure that includes a hydrophilic inside shell and a hydrophobic outside layer. Consequently, the two silica-based nanoparticles were expected to present differential MB loading. It should also be noted that MB is known to aggregate, particularly at high concentrations or when adsorbed into oppositely charged interfaces (7,43,44). As observed in Fig. 3, the spectrum of the MB-loaded sol–gel silica nanoparticles has the most noticeable peak at 600 nm, typical of MB dimers. Therefore, in addition to monomers, MB exhibits some

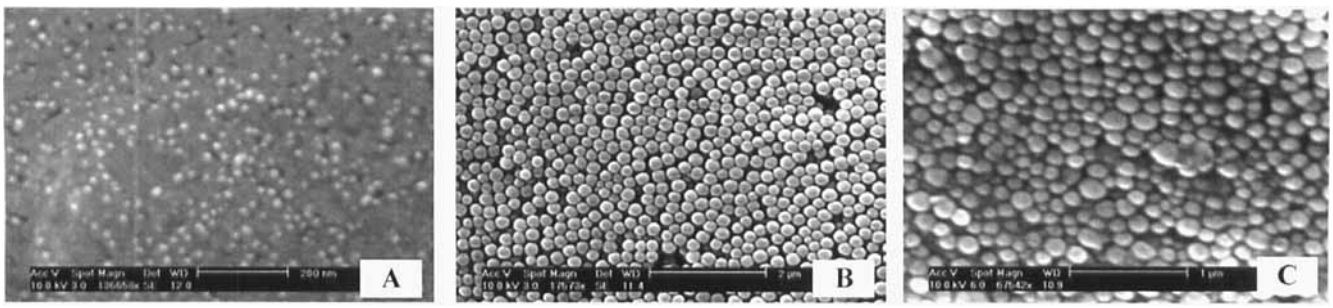


**Figure 4.** SEM images of three types of MB-loaded nanoparticles: (A) polyacrylamide nanoparticles, (B) sol–gel silica nanoparticles and (C) ORMOSIL nanoparticles. Scale bars: 200 nm, 2 μm and 1 μm, respectively.

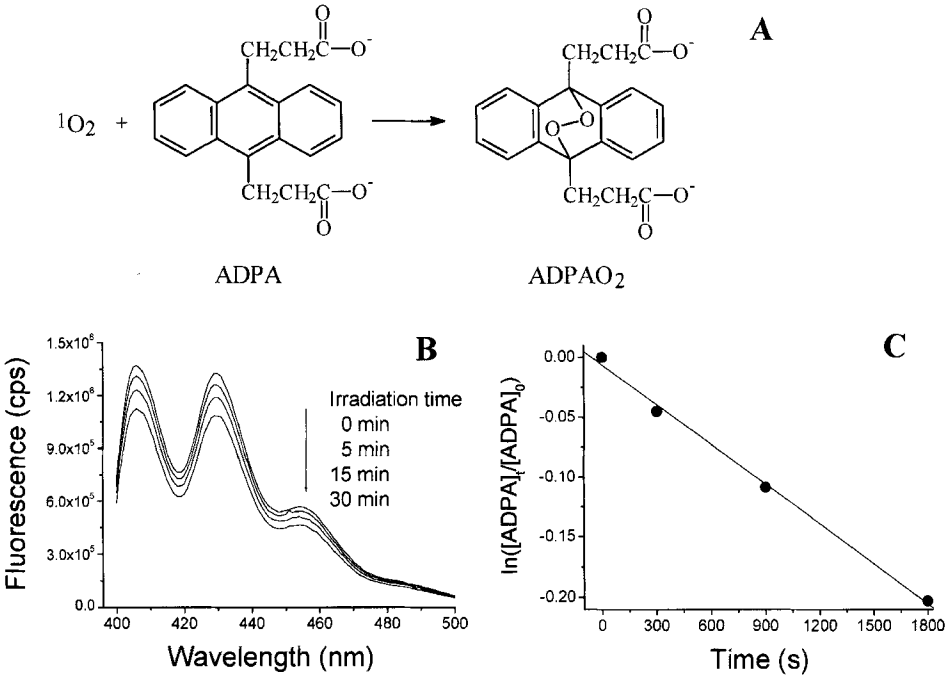


**Figure 5.** (A) Reaction of ADPA with $^1O_2$ to form the nonfluorescent endoperoxide ADPAO$_2$. (B) Fluorescence spectra of the mixture of 1 mg/mL MB-loaded polyacrylamide nanoparticles and ADPA, after irradiation at 650 nm for 0, 5, 15 and 30 min. (C) The best fit of Eq. 6 to the experimental points of the same sample, where the value of $k$ obtained was $1.1 \times 10^{-4}$/s.

dimerization in nanoparticles, which can influence the efficiency of $^1O_2$ generation.

### $^1O_2$ detection by ADPA

As described previously, a chemical test for $^1O_2$ production was carried out to compare the different matrix effects on the delivery of $^1O_2$. During these experiments, the fluorescence intensity of ADPA continuously decreased as the mixtures of ADPA with different MB formulations were irradiated at 650 nm. The decrease in fluorescence indicated the production of $^1O_2$, which irreversibly reacted with ADPA. As an example, typical results obtained from a suspension of 1 mg/mL MB-loaded polyacrylamide nanoparticles are represented in Fig. 5. Assuming a linear dependence, the concentration of ADPA can be calculated from the fluorescence intensity. The best fit of Eq. 6 to the experimental data is also shown, and the value of $k$ obtained is $1.1 \times 10^{-4}$/s.

According to the kinetic scheme derived above, ideally, the normalized rate constant $k'$ should be proportional to $\Phi$, the quantum yield of $^1O_2$, after normalization to $I^{abs}$ under the same experimental conditions. As shown in Fig. 6, the normalized $k'$ of the MB-loaded polyacrylamide nanoparticles is the closest to that of free MB dye, followed in sequence by that of the MB-loaded ORMOSIL nanoparticles and the sol–gel silica nanoparticles. However, caution is required in the interpretation of the $k'$ values of the nanoparticles obtained from the rate of consumption of ADPA, as compared with that of the free dye. As discussed previously (40,41), the $k'$ values cannot be directly translated into differences in terms of the quantum yield of $^1O_2$ production because the matrix may affect the rate constant in a variety of ways that were not evaluated and remain to be determined. In our case, the $k'$ values only indicate that the delivery of $^1O_2$ is reduced to different extents by the encapsulation of MB in nanoparticles. This difference in activity may be partially attributed to the various microenvironments in the nanoparticles, in particular, the local sequestration of produced $^1O_2$ by the matrices. Moreover, as mentioned in the previous section, MB forms dimers in nanoparticles, which do not absorb light at 650 nm to produce $^1O_2$. Thus, despite the normalization to $I^{abs}$ of the MB monomers, the influence of dimerization on the $k'$ value may be a complicating factor.

On the other hand, the value of the normalized rate constant $k'$ alone is not fully representative of the efficiency of the three MB-loaded nanoparticles. By accounting for the loading of MB, the relative $^1O_2$ delivery per milligram of each type of nanoparticle can be compared. First, the sol–gel silica nanoparticles are not necessarily the worst choice. Despite the low $k'$ value, their $^1O_2$ delivery per milligram of the nanoparticle is 3.5 times larger than that of the polyacrylamide nanoparticles because of their remarkable MB loading. Second, the ORMOSIL nanoparticles, until now, provide the second best results in terms of MB loading and delivery efficiency of $^1O_2$, resulting in 1.9 times more $^1O_2$ delivery per milligram of the nanoparticle compared with that of the polyacrylamide nanoparticles. Further investigations of this unique double-shell matrix may be of interest. Finally, the polyacrylamide nanoparticles demonstrate the most efficient delivery of $^1O_2$ per MB molecule by having the highest $k'$ among these three nanoparticles, but their $^1O_2$ delivery per milligram of nanoparticle is the least significant due to their low MB loading. However, these nanoparticles give the most stable aqueous suspension, which facilitates the subsequent *in vitro* PDT tests.

### *In vitro* PDT studies

With the intention of confirming the photodynamic cytotoxicity of the nanoparticle formulations, preliminary *in vitro* PDT tests were performed on rat C6 glioma tumor cells with MB-loaded polyacrylamide nanoparticles.

Confocal microscopy was used to obtain a series of images of cells treated with polyacrylamide nanoparticles under red light irradiation. The treated samples also contained calcein AM and PI to monitor live and dead cells, respectively. Figure 7 shows typical confocal images (calcein and PI channels overlaid) of cells treated

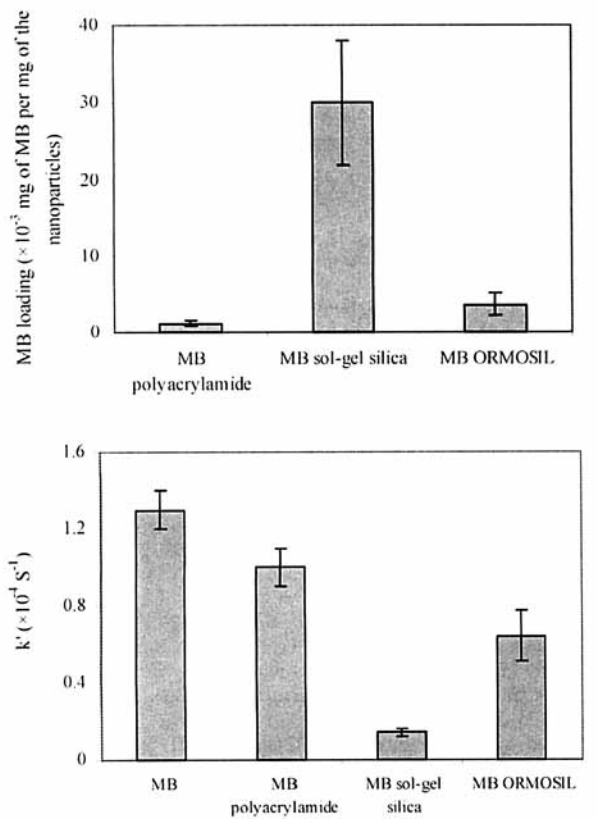


**Figure 6.** The loading of MB (top) and the normalized rate constant $k'$ recovered from experimental data for three types of MB-loaded nanoparticles ($k' = k/(I^{abs}/I^0)$, $I^0$ is the light absorbed by 1 mg/mL MB-loaded polyacrylamide nanoparticles) (bottom).

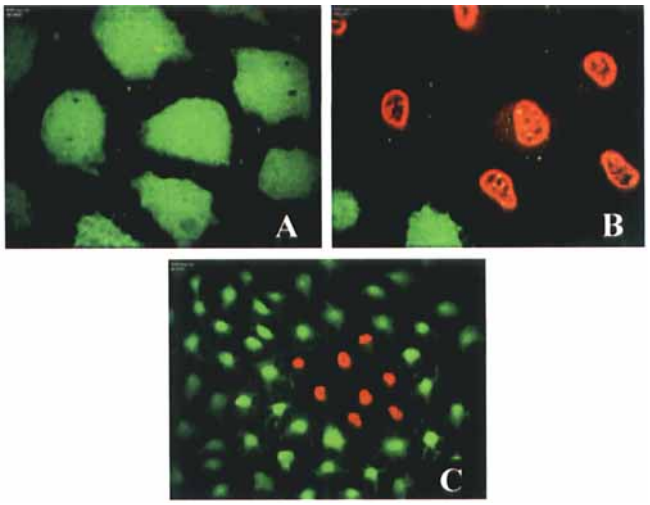


**Figure 7.** Confocal images (calcein [green] and PI [red] channels are both shown) of rat C6 glioma tumor cells treated with 1 mg/mL MB-loaded polyacrylamide nanoparticles: (A) before light exposure, taken with a 60× objective; (B) 2 h after 5 min light exposure, taken with a 60× objective and (C) 2 h after 5 min light exposure, taken with a 20× objective, showing that cell death is limited to laser irradiated areas.

with 1 mg/mL MB-loaded polyacrylamide nanoparticles, equivalent to 0.3 μ*M* MB. Before light irradiation, all the cells in Fig. 7A were stained by calcein showing green fluorescence, which verified the cell viability. The image in Fig. 7B was taken 2 h after 5 min irradiation at 647 nm using a 60× objective. The cytoplasm of the cultured cells lost its green fluorescence in a time-dependent manner. Concomitant with the loss of calcein, the nuclei of the compromised cells were observed to increase their incorporation of PI, indicated by the red fluorescence. Internal controls were obtained by capturing images sequentially, using a 20× objective with the irradiated area in the center (Fig. 7C). Local illumination induced death of only those cells located in the beam of light; whereas other cells, in contact with MB-loaded nanoparticles but not illuminated by the laser, remained intact, represented by green fluorescence. These observations suggest that only the exposure of cells to the combination of MB-loaded nanoparticles and light resulted in the production of sufficient quantities of $^1O_2$ to damage and kill cancer cells in culture.

Two other control experiments were carried out to verify the photocytotoxicity of the MB-loaded polyacrylamide nanoparticles (data not presented here): one was performed without MB-loaded nanoparticles but with red light irradiation under the same conditions, the other was carried out with blank polyacrylamide nanoparticles (not MB loaded) and light exposure. Neither revealed significant cell death in the illumination area. Therefore, neither the red light nor the polyacrylamide matrix by itself is cytotoxic to tumor cells; both light and the PS, in combination, are required for photodynamic cytotoxicity.

To compare the photodynamic properties of free MB with MB-loaded nanoparticles, two additional tests were conducted using free MB under the same *in vitro* experimental conditions used for nanoparticles. The first C6 glioma cell sample was incubated overnight with an equivalent amount of free MB to that of 1 mg/mL MB-loaded polyacrylamide nanoparticles. Then excess MB that was not taken up by the cells was washed away before the experiment. The second sample was prepared with a direct addition of the same amount of free MB without incubation. On light illumination, both exhibited minimal cell death (data not presented here).

However, the photodynamic mechanism of free PS is fundamentally different from the work presented in this article. Incubation is not necessary for the nanoparticles because they are not designed to internalize into target cells but to deliver $^1O_2$ thus requiring only external contact with the cell membrane. Furthermore, the nanoparticle matrix protects the entrapped PS from the biological environment. In the case of nonencapsulated MB, the diminished phototoxic effect could be primarily attributed to the reduction of the free MB to LMB, the nonphotoactive form. The aggregation of free PS molecules and their being pumped back out of the cells by MDR mechanisms may also cause severe problems in practical PDT. On the contrary, our drug-loaded nanoparticles should be able to minimize these complications often encountered with free dyes, thus resulting in higher cell killing efficiency.

In summary, these preliminary studies demonstrated effective *in vitro* photodynamic activity with one matrix, *i.e.* polyacrylamide nanoparticles. In the future we expect that the delivering matrix will facilitate the systemic administration of MB, on the basis of the successful *in vivo* PDT tests reported recently using the polyacrylamide nanoparticles loaded with Photofrin (29). Although the current data are insufficient to draw a firm quantitative conclusion on how much the nanoparticle formulation enhances the efficacy of PDT, compared with the free PS, there is no doubt that it is by a significant factor. In addition, not all aspects of the photocytotoxicity observed with the MB-loaded polyacrylamide nanoparticles have been fully examined. For example, photoinduced damage in traditional PDT can lead to either necrotic or apoptotic

cell death (45–47). Although the balance between apoptosis and necrosis should also be dependent on many other features, such as the dose of PDT and the cell type, in this case the use of the DNP may favor necrosis (R. Schneider and M. A. Philbert, personal communication) by delivering only $^1O_2$ to the adjacent cell membranes. A better understanding of the cell death mechanism with this protocol may provide an additional insight and serve as a guide for further development of this DNP for PDT applications.

## CONCLUSIONS

In this study, a novel design of nanoplatforms using MB for PDT has been developed. It provides a stable PS-loaded formulation and delivers $^1O_2$ from the outside of the tumor cells. It has been demonstrated that MB, which has been limited to topical treatment in PDT because of its varying behavior *in vivo*, can be incorporated into different types of nanoparticles, including polyacrylamide, sol–gel silica and ORMOSIL. In addition, on light irradiation, the encapsulated MB is able to generate sufficient $^1O_2$ that can diffuse out of the matrix, reach the adjacent cell membranes and kill the tumor cell. These results suggest that there is a significant potential for clinical PDT applications of this low-toxicity PS when encapsulated in a DNP. The efficiency of delivering $^1O_2$ from these nanoparticles was also determined by the ADPA method and was compared for different nanoparticle matrices. To date, MB-loaded polyacrylamide nanoparticles exhibit the most promising properties with respect to the efficiency of $^1O_2$ delivery, particle size and particle suspendability. On the other hand, the two silica-based nanoparticles, sol–gel silica and ORMOSIL, are characterized by a number of intriguing properties and are worth additional investigation. Furthermore, preliminary *in vitro* PDT experiments carried out on rat C6 glioma tumor cells using MB-loaded polyacrylamide nanoparticles revealed significant photodynamic cytotoxicity. Although only simple MB-loaded nanoparticles, *i.e.* unconventional but single-function PS-carrier systems, are reported in this article, study is under way to add the functions of plasma residence time control (by PEGylation), tumor cell targeting and on-site MRI detection (using contrast enhancing agents) to complete the multifunctional DNP design.

*Acknowledgements*—This study has been supported by NCI contract N01-CO-37123 as well as NIH grants 8RO1-EB00250-0909 (R.K.) and ES08846 (M.A.P.). The authors would like to thank Dr. Murphy Brasuel, Dr. Yong-Eun Lee Koo and Edwin Park for their advice and assistance and Dr. Eric Monson for the graphics of Fig. 2. The Electron Microbeam Analysis Laboratory at the University of Michigan is also gratefully acknowledged for the use of the SEM.

## REFERENCES

1. MacDonald, I. J. and T. J. Dougherty (2001) Basic principles of photodynamic therapy. *J. Porphyr. Phthalocyanines* **5**, 105–129.
2. Dougherty, T. J., C. J. Gomer, B. W. Henderson, G. Jori, D. Kessel, M. Korbelik, J. Moan and Q. Peng (1998) Photodynamic therapy. *J. Natl. Cancer Inst.* **90**, 889–905.
3. Schuitmaker, J. J., P. Bass, H. vanLeengoed, F. W. vanderMeulen, W. M. Star and N. vanZandwijk (1996) Photodynamic therapy: a promising new modality for the treatment of cancer. *J. Photochem. Photobiol. B: Biol.* **34**, 3–12.
4. Sharman, W. M., C. M. Allen and J. E. van Lier (1999) Photodynamic therapeutics: basic principles and clinical applications. *Drug Discov. Today* **4**, 507–517.
5. Dolmans, D., D. Fukumura and R. K. Jain (2003) Photodynamic therapy for cancer. *Nat. Rev. Cancer* **3**, 380–387.
6. Bonnett, R. (1995) Photosensitizers of the porphyrin and phthalocyanine series for photodynamic therapy. *Chem. Soc. Rev.* **24**, 19–33.
7. Gabrielli, D., E. Belisle, D. Severino, A. J. Kowaltowski and M. S. Baptista (2004) Binding, aggregation and photochemical properties of methylene blue in mitochondrial suspensions. *Photochem. Photobiol.* **79**, 227–232.
8. Redmond, R. W. and J. N. Gamlin (1999) A compilation of singlet oxygen yields from biologically relevant molecules. *Photochem. Photobiol.* **70**, 391–475.
9. DeRosa, M. C. and R. J. Crutchley (2002) Photosensitized singlet oxygen and its applications. *Coord. Chem. Rev.* **233**, 351–371.
10. Mellish, K. J., R. D. Cox, D. I. Vernon, J. Griffiths and S. B. Brown (2002) *In vitro* photodynamic activity of a series of methylene blue analogues. *Photochem. Photobiol.* **75**, 392–397.
11. Tuite, E. M. and J. M. Kelly (1993) Photochemical interactions of methylene blue and analogs with DNA and other biological substrates. *J. Photochem. Photobiol. B: Biol.* **21**, 103–124.
12. Orth, K., A. Ruck, A. Stanescu and H. G. Beger (1995) Intraluminal treatment of inoperable esophageal tumors by intralesional photodynamic therapy with methylene blue. *Lancet* **345**, 519–520.
13. Wainwright, M. (1996) Non-porphyrin photosensitizers in biomedicine. *Chem. Soc. Rev.* **25**, 351–359.
14. Williams, J. L., J. Stamp, R. Devonshire and G. J. S. Fowler (1989) Methylene blue and the photodynamic therapy of superficial bladder-cancer. *J. Photochem. Photobiol. B: Biol.* **4**, 229–232.
15. Orth, K., G. Beck, F. Genze and A. Ruck (2000) Methylene blue mediated photodynamic therapy in experimental colorectal tumors in mice. *J. Photochem. Photobiol. B: Biol.* **57**, 186–192.
16. Wainwright, M., D. A. Phoenix, L. Rice, S. M. Burrow and J. Waring (1997) Increased cytotoxicity and phototoxicity in the methylene blue series via chromophore methylation. *J. Photochem. Photobiol. B: Biol.* **40**, 233–239.
17. Konan, Y. N., R. Gurny and E. Allemann (2002) State of the art in the delivery of photosensitizers for photodynamic therapy. *J. Photochem. Photobiol. B: Biol.* **66**, 89–106.
18. Wang, S. Z., R. M. Gao, F. M. Zhou and M. Selke (2004) Nanomaterials and singlet oxygen photosensitizers: potential applications in photodynamic therapy. *J. Mater. Chem.* **14**, 487–493.
19. Labib, A., V. Lenaerts, F. Chouinard, J. C. Leroux, R. Ouellet and J. E. Vanlier (1991) Biodegradable nanospheres containing phthalocyanines and naphthalocyanines for targeted photodynamic tumor-therapy. *Pharm. Res.* **8**, 1027–1031.
20. Lenaerts, V., A. Labib, F. Chouinard, J. Rousseau, H. Ali and J. Vanlier (1995) Nanocapsules with a reduced liver uptake—targeting of phthalocyanines to Emt-6 mouse mammary-tumor *in-vivo*. *Eur. J. Pharm. Biopharm.* **41**, 38–43.
21. Konan, Y. N., M. Berton, R. Gurny and E. Allemann (2003) Enhanced photodynamic activity of meso-tetra(4-hydroxyphenyl)porphyrin by incorporation into sub-200 nm nanoparticles. *Eur. J. Pharm. Sci.* **18**, 241–249.
22. Konan, Y. N., R. Cerny, J. Favet, M. Berton, R. Gurny and E. Allemann (2003) Preparation and characterization of sterile sub-200 nm meso-tetra(4-hydroxylphenyl)porphyrin-loaded nanoparticles for photodynamic therapy. *Eur. J. Pharm. Biopharm.* **55**, 115–124.
23. Konan, Y. N., J. Chevallier, R. Gurny and E. Allemann (2003) Encapsulation of p-THPP into nanoparticles: cellular uptake, subcellular localization and effect of serum on photodynamic activity. *Photochem. Photobiol.* **77**, 638–644.
24. Roy, I., T. Y. Ohulchanskyy, H. E. Pudavar, E. J. Bergey, A. R. Oseroff, J. Morgan, T. J. Dougherty and P. N. Prasad (2003) Ceramic-based nanoparticles entrapping water-insoluble photosensitizing anticancer drugs: a novel drug-carrier system for photodynamic therapy. *J. Am. Chem. Soc.* **125**, 7860–7865.
25. Harrell, J. A. and R. Kopelman (2000) Biocompatible probes measure intracellular activity. *Biophotonics Int.* **7**, 22–24.
26. Monson, E., M. Brasuel, M. A. Philbert and R. Kopelman (2003) PEBBLE nanosensors for in vitro bioanalysis. Chap. 59. In *Biomedical Photonics Handbook* (Edited by T. Vo-Dinh), pp. 1–14. CRC Press, New York.
27. Xu, H., S. M. Buck, R. Kopelman, M. A. Philbert, M. Brasuel, B. Ross and A. Rehemtulla (2004) Photo-excitation based nano-explorers: chemical analysis inside live cells and photodynamic therapy. *Jortner Festschrift, Isr. J. Chem.* **44**, 317–337.
28. Xu, H., S. M. Buck, R. Kopelman, M. A. Philbert, M. Brasuel, E. Monson, C. Behrend, B. Ross, A. Rehemtulla and Y.-E. L. Koo (2004) Fluorescent PEBBLE nanosensors and nanoexplorers for real-

time intracellular and biomedical applications. Chap. 10. In *Topics in Fluorescence Spectroscopy* (Edited by C. D. Geddes and J. R. Lakowicz). Kluwer Academic/Plenum Press, New York. (In press)
29. Ross, B., A. Rehemtulla, Y.-E. L. Koo, R. Reddy, G. Kim, C. Behrend, S. Buck, R. J. Schneider II, R. Weissleder, M. A. Philbert and R. Kopelman (2004) Photonic and magnetic nanoexplorers for biomedical use: from subcellular imaging to cancer diagnostics and therapy. *SPIE Proc.* **5331**, 76–83.
30. Moffat, B. A., R. G. Reddy, P. McConville, D. E. Hall, T. L. Chenevert, R. Kopelman, M. A. Philbert, R. Weissleder, A. Rehemtulla and B. Ross (2003) A novel polyacrylamide magnetic nanoparticle contrast agent for molecular imaging using MRI. *J. Mol. Imaging* **2**, 1–9.
31. Levy, L., Y. Sahoo, K. S. Kim, E. J. Bergey and P. N. Prasad (2002) Nanochemistry: synthesis and characterization of multifunctional nanoclinics for biological applications. *Chem. Mater.* **14**, 3715–3721.
32. Xu, H., F. Yan, E. E. Monson and R. Kopelman (2003) Room-temperature preparation and characterization of poly (ethylene glycol)-coated silica nanoparticles for biomedical applications. *J. Biomed. Mater. Res.* **66A**, 870–879.
33. Leroux, J. C., E. Doelker and R. Gurny (1996) The use of drug-loaded nanoparticles in cancer chemotherapy. In *Microencapsulation Methods and Industrial Application* (Edited by S. Benita), pp. 535–575. Marcel Dekker, New York.
34. Clark, H. A., M. Hoyer, M. A. Philbert and R. Kopelman (1999) Optical nanosensors for chemical analysis inside single living cells. 1. Fabrication, characterization, and methods for intracellular delivery of PEBBLE sensors. *Anal. Chem.* **71**, 4831–4836.
35. Park, E. J., M. Brasuel, C. Behrend, M. A. Philbert and R. Kopelman (2003) Ratiometric optical PEBBLE nanosensors for real-time magnesium ion concentrations inside viable cells. *Anal. Chem.* **75**, 3784–3791.
36. Stöber, W., A. Fink and E. Bohn (1968) Controlled growth of monodisperse silica spheres in micron size range. *J. Colloid Interface Sci.* **26**, 62–69.
37. Xu, H., J. W. Aylott, R. Kopelman, T. J. Miller and M. A. Philbert (2001) A real-time ratiometric method for the determination of molecular oxygen inside living cells using sol-gel-based spherical optical nanosensors with applications to rat C6 glioma. *Anal. Chem.* **73**, 4124–4133.
38. Koo, Y.-E. L., Y. Cao, R. Kopelman, S. M. Koo, M. Brasuel and M. A. Philbert (2004) Real-time measurements of dissolved oxygen inside live cells by organically modified silicate fluorescent nanosensors. *Anal. Chem.* **76**, 2498–2505.
39. Hah, H. J., J. S. Kim, B. J. Jeon, S. M. Koo and Y. E. Lee (2003) Simple preparation of monodisperse hollow silica particles without using templates. *Chem. Commun.* 1712–1713.
40. Moreno, M. J., E. Monson, R. G. Reddy, A. Rehemtulla, B. D. Ross, M. A. Philbert, R. J. Schneider and R. Kopelman (2003) Production of singlet oxygen by $Ru(dpp(SO_3)_2)_3$ incorporated in polyacrylamide PEBBLES. *Sens. Actuators B: Chem.* **90**, 82–89.
41. Yan, F. and R. Kopelman (2003) The embedding of meta-tetra(hydroxyphenyl)-chlorin into silica nanoparticle platforms for photodynamic therapy and their singlet oxygen production and pH-dependent optical properties. *Photochem. Photobiol.* **78**, 587–591.
42. Niedre, M., M. S. Patterson and B. C. Wilson (2002) Direct near-infrared luminescence detection of singlet oxygen generated by photodynamic therapy in cells *in vitro* and tissues *in vivo*. *Photochem. Photobiol.* **75**, 382–391.
43. Severino, D., H. C. Junqueira, M. Gugliotti, D. S. Gabrielli and M. S. Baptista (2003) Influence of negatively charged interfaces on the ground and excited state properties of methylene blue. *Photochem. Photobiol.* **77**, 459–468.
44. Junqueira, H. C., D. Severino, L. G. Dias, M. S. Gugliotti and M. S. Baptista (2002) Modulation of methylene blue photochemical properties based on adsorption at aqueous micelle interfaces. *Phys. Chem. Chem. Phys.* **4**, 2320–2328.
45. Oleinick, N. L., R. L. Morris and T. Belichenko (2002) The role of apoptosis in response to photodynamic therapy: what, where, why, and how. *Photochem. Photobiol. Sci.* **1**, 1–21.
46. Ball, D. J., Y. Luo, D. Kessel, J. Griffiths, S. B. Brown and D. I. Vernon (1998) The induction of apoptosis by a positively charged methylene blue derivative. *J. Photochem. Photobiol. B: Biol.* **42**, 159–163.
47. Noodt, B. B., G. H. Rodal, M. Wainwright, Q. Peng, R. Horobin, J. M. Nesland and K. Berg (1998) Apoptosis induction by different pathways with methylene blue derivative and light from mitochondrial sites in V79 cells. *Int. J. Cancer* **75**, 941–948.